Feasibility and Mechanistic Analysis of 3-Stack Aluminium-Steel Spot Joints Using Vaporizing Foil Actuator Welding with Partial Pre-Forming

D. Kumar[1], J. Choi[1], H. Lim[1], H. Kwon[2], J. Jeong[2], T. Lee[1,*]

[1] Department of Mechanical Engineering, Incheon National University, Republic of Korea
[2] R&D Division, Hyundai Motor Company, Republic of Korea
*Corresponding author. Email: taelee19@inu.ac.kr

Abstract

The advancement of spot joining techniques is crucial for automotive manufacturing, yet integrating aluminum-steel (Al-Fe), combinations presents inherent challenges. Traditional methods, such as resistance spot welding (RSW), often lead to the formation of brittle intermetallic compounds (IMCs) and residual stresses, compromising joint integrity. Innovative strategies that enhance mechanical performance while optimizing weight are essential for multi-material assemblies. Advanced techniques like vaporizing foil actuator welding (VFAW) offer a promising solution, enabling metallurgical bonding with minimal heat-induced damage, thereby reducing residual stresses and improving structural reliability. This study investigates the feasibility of fabricating a 3-stack (Al-Fe-Fe) spot joint using VFAW, employing partial pre-forming of intermediate plates to achieve single-step joining. Smoothed particle hydrodynamics (SPH) modeling is applied to analyze transient stress wave propagation and interfacial jetting dynamics, elucidating their mechanistic influence on interfacial bond formation during high-speed multi-plate interactions. The findings underscore the critical role of partial pre-forming in enabling successful 3-stack VFAW joints.

Keywords

Vaporizing foil actuator welding (VFAW), Al/Steel, 3-stack, Process-property relationship, SPH

1 Introduction

The integration of aluminum and steel in automotive manufacturing offers significant advantages in achieving lightweight, high-strength structures (Yang et al., 2024). Dominantly, joining techniques such as resistance spot welding (RSW) are used in the industry; however, faces significant challenges, primarily due to the formation of brittle intermetallic compounds (IMCs) at the joint interface, which compromises mechanical performance (Shi et al., 2025, Kumar et al., 2024). Additionally, disparities in melting points and thermal conductivities between aluminum and steel exacerbate welding difficulties (Kulkarni et al., 2022).

Three-stack or multi-stack joints involving layered combinations of aluminum and steel are particularly relevant for automotive applications due to their ability to integrate lightweight and high-strength materials efficiently. However, achieving reliable multi-stack joints remains challenging due to uneven stress distribution and potential defects such as cracks or delamination (Shi et al., 2023). Traditional methods like RSW often struggle with such configurations, leading to inconsistent joint quality (Achira et al., 2022, Brechelt et al., 2020). To address these challenges, advanced joining techniques like VFAW are being explored for their potential to minimize thermal effects while maintaining joint integrity.

Vaporizing Foil Actuator Welding (VFAW) emerges as a compelling alternative, utilizing high-voltage (current) pulses (100–150 kA) to sublimate an aluminum foil, creating high-pressure plasma pulse to propel flyer metal plates into collision with target metal, at high velocities (300–1500 m/s) and oblique angles (5–20 degrees), facilitating solid-state bonding without significant thermal input (Vivek et al., 2013, Kapil et al., 2025). This process effectively minimizes IMC formation, thereby enhancing joint integrity (Kumar et al., 2025).

To elucidate the underlying mechanisms of VFAW and optimize the process parameters for specific applications, Smoothed Particle Hydrodynamics (SPH) modeling serves as a robust analytical tool. Its mesh-free nature adeptly captures the high strain rates and complex interfacial phenomena inherent in VFAW, providing critical insights into stress wave propagation and jetting dynamics during the welding process.

Previously, some researchers (Mao et al., 2021, Kapil et al., 2020 and Li et al., 2021) have already utilized VFAW for a multi-stack configuration. As Mao et al., 2021, demonstrated that using a thin Al 3003-H14 interlayer between thick aluminum alloy 5754 and HSLA 340 steel achieved robust joints with reduced IMC formation due to controlled energy dissipation. Similar studies by Li et al., 2021 on heat treatment of interlayers revealed that treating the interlayer material can stabilize the microstructure, thereby improving mechanical properties and fatigue resistance. Furthermore, Kapil et al., 2020 highlighted that employing interlayers in VFAW not only aids in energy absorption during high-velocity impacts but also helps prevent localized melting, thereby maintaining joint quality and structural integrity. However, in all these studies, the middle layer was significantly thinner than both the flyer and target plates, primarily serving as an interlayer rather than a structural component.

Therefore, this study aims to investigate the feasibility of fabricating multi-stack aluminum-steel-steel spot joints using VFAW, with an emphasis on partial pre-forming technique where all three plates have comparable thickness and the middle layer functions as a structural component rather than merely an interlayer. This approach addresses the challenges associated with achieving consistent bonding and mechanical integrity in multi-layer configurations. Through comprehensive SPH modeling, the study will analyze stress distributions, interfacial dynamics and the influence of joint geometry on joint quality. The insights gained from the analytical model combined with SPH simulations are expected to guide process optimization, advancing the application of VFAW in producing robust, lightweight automotive structures, particularly where multi-material integration is critical.

2 Methodology

2.1 Materials and methods

The selected materials include an A6451P-T4 aluminum alloy flyer plate with a thickness of 1.5 mm, chosen for its lightweight properties, formability, and structural performance, making it suitable for automotive applications (Kumar et al., 2025). The intermediate plate, as well as the target plate, consists of SPCC (General purpose cold-rolled carbon steel) steel with a thickness of 0.8 mm, where the intermediate plate acts as a structural component to enhance joint strength and stability (Liu et al., 2025). The mechanical properties and chemical composition of the materials are shown in Table 1. An aluminium foil actuator with a thickness of 0.0762 mm serves as the vaporizing medium, positioned parallel to the weld axis to ensure consistent acceleration during the welding process.

The VFAW process was conducted using the APPLIED IMPULSE INC.® CIS-6 system with a maximum capacity of 6 kJ, as shown in Fig. 1 (a). The experimental setup involved arranging the three plates in a pre-formed configuration to accommodate rapid flyer acceleration and minimize initial resistance (Fig. 1(b)).

Partial pre-forming (i.e. forming to a depth lower than the pre-forming of the target plate) of the intermediate steel plate was employed to create a controlled gap, enabling efficient collision dynamics and uniform stress distribution during welding. This setup aimed to address the challenges of achieving consistent bonding when the intermediate layer functions as a structural component rather than just an interlayer (Fig. 1 (c-d)).

During the welding process, the aluminum actuator foil rapidly vaporizes, generating a high-pressure plasma pulse that propels the A6451P-T4 flyer towards the pre-formed SPCC intermediate plate. The initial impact occurs between the flyer and the intermediate layer, followed by a secondary impact between the intermediate and target layers. The use of a structurally comparable intermediate plate rather than a typical interlayer ensures that the joint can withstand higher mechanical loads while maintaining robust bonding and load transfer.

SPH modeling was conducted to model the dynamic interaction between the flyer, intermediate, and target plates. The model analyzed stress wave propagation, and interfacial

jetting phenomena, focusing on how the comparable thickness of the intermediate layer influences the bond quality compared to configurations with thinner interlayers (Mao et al., 2021). The simulations aimed to elucidate the mechanistic role of partial pre-forming in achieving effective metallurgical bonding in multi-stack joints.

***Table 1**: Mechanical properties and chemical composition of the workpiece material*

	Mechanical Properties			Chemical Compositions (At%)					
Material	YP (MPa)	TS (MPa)	EL (%)	Fe	C	Mn	Si	Mg	Al
SPCC	176	298	50	Bal.	0.003	0.08	0.002	-	-
A6451P-T4	136.6	266.1	28.7	0.17	-	0.072	1.1	0.52	Bal.

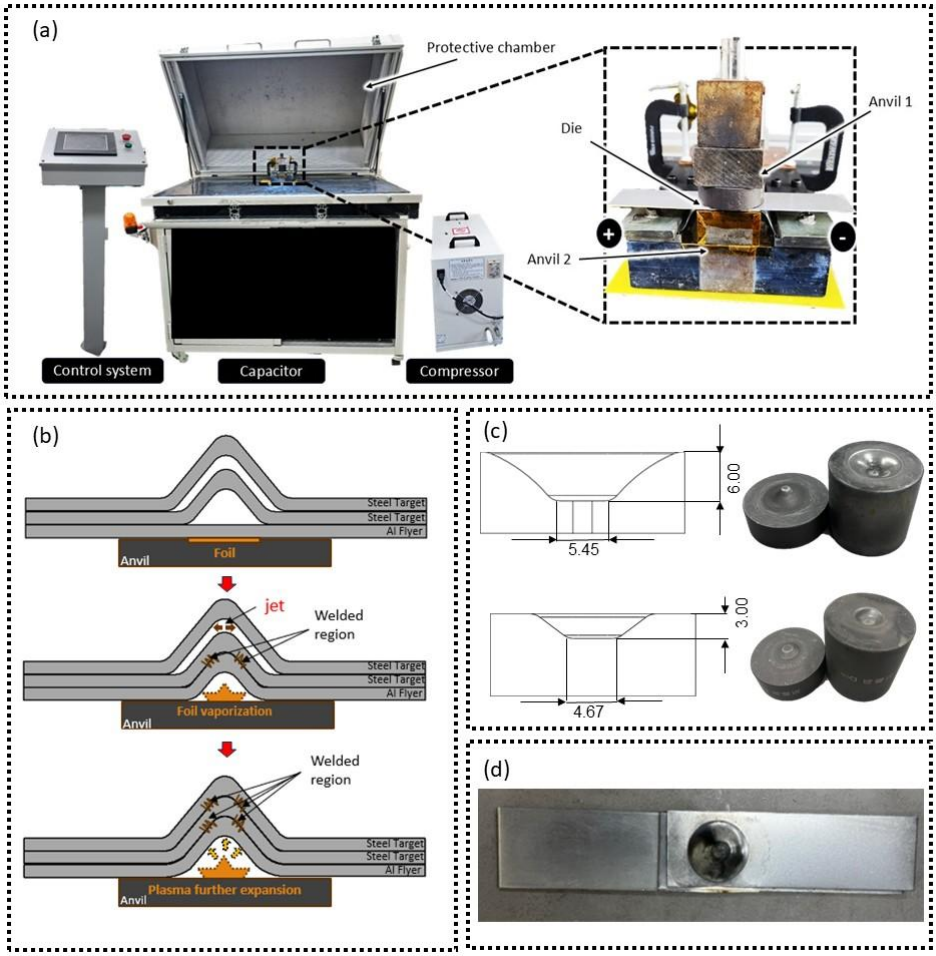

***Figure 1**: Pictorial representation of (a) working setup of VFAW, (b) welding process, (c) die design used during preforming and partial preforming and (d) experimentally obtained Al-Fe-Fe VFAW welded sample*

2.2 Analytical modeling

In this one-dimensional (1-D) analytical approach, Plate 1 (flyer) is accelerated and impacts Plate 2 (intermediate), which is deformable, of comparable thickness, and initially unsupported, consistent with the experimental configuration. Following this, the intermediate plate deforms and travels across a finite standoff distance to impact Plate 3 (target), which is rigidly backed. This configuration divides the modelling into two sequential impact events synonymous with the experiments.

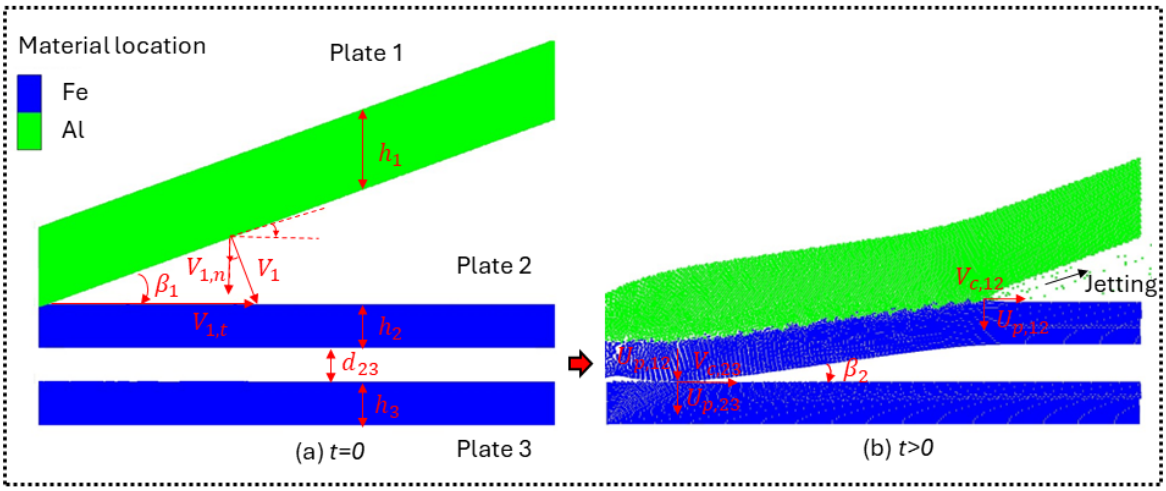

***Figure 2**: Pictorial representation of oblique impact at (a) interface 1 and (b) interface 2*

2.2.1 Interface 1: flyer (plate 1) → intermediate (plate 2)

When Plate 1 impacts Plate 2 obliquely at an angle β_1, shock waves are generated on both plates. The velocity components of the flyer in the normal and tangential directions are given by,

$$V_{1,n} = V_1 \sin\beta_1 \, , V_{1,t} = V_1 \cos\beta_1, V_{2,n} = 0 \tag{1}$$

Applying the two-sided Rankine-Hugoniot relations equating pressure and particle velocities,

$$P_1 = P_2 = P_{int1}, U_{p,1} = U_{p,2} = U_{p,int1}. \tag{2}$$

$$P_1 = \rho_1\left(C_{01} + S_1 U_{P,1}\right)U_{P,1}, P_2 = \rho_2\left(C_{02} + S_2 U_{P,2}\right)U_{P,2}. \tag{3}$$

At interface 1, $P_1 = P_2$ and $U_{p,1} = U_{p,2} = U_{p,12}$ (shared particle velocity). As they are no longer symmetric, and both plates move post-impact. Applying conservation of momentum and mass,

$$\rho_1(C_{01} + S_1U_P)U_{P,12} = \rho_2\big(C_{02} + S_2U_{P,12}\big)U_{P,12} \tag{4}$$

$$\rho_1\big(C_{01} + S_1U_{P,12}\big) = \rho_2\big(C_{02} + S_2U_{P,12}\big) \tag{5}$$

$$U_{P,12} = \frac{\rho_2C_{02} - \rho_1C_{01}}{(\rho_1S_1 - \rho_2S_2)} \tag{6}$$

$$\text{Or using impedance, } U_{P,12} = V_i\frac{Z_2 - Z_1}{Z_1 + Z_2},\ Z_i = \rho_iC_{0i} \tag{7}$$

This provides the impact-driven interface velocity in terms of material impedances. The resulting shock velocities in the flyer and intermediate plate are given by,

$$U_{s1} = C_{01} + S_1U_P = C_{01} + S_1\frac{\rho_2C_{02} - \rho_1C_{01}}{\rho_1S_1 - \rho_2S_2} = \frac{\rho_2(S_1C_{02} - S_2C_{01})}{\rho_1S_1 - \rho_2S_2} \tag{8}$$

$$U_{s2} = C_{02} + S_2\frac{\rho_2C_{02} - \rho_1C_{01}}{\rho_1S_1 - \rho_2S_2} = \frac{\rho_1(S_1C_{02} - S_2C_{01})}{\rho_1S_1 - \rho_2S_2} \tag{9}$$

This captures the oblique shock propagation in both plates. However, as both plates are deformable with a comparable thickness, the shock reflects from the rear faces of both plates and returns towards interface 1. Their respective arrival times at the interface 1 are,

$$t_1^* = \frac{2h_1}{U_{s1}\cos\beta_1} = \frac{2h_1(\rho_1S_1 - \rho_2S_2)}{\rho_2(S_1C_{02} - S_2C_{01})\cos\beta_1} \tag{10}$$

$$t_2^* = \frac{2h_2}{U_{s2}\cos\beta_1} = \frac{2h_2(\rho_1S_1 - \rho_2S_2)}{\rho_1(S_1C_{02} - S_2C_{01})\cos\beta_1} \tag{11}$$

The earlier of the two times will dictate the potential interference with melt solidification, i.e., weld failure by dynamic solidification cracking which occurs when a reflected shock wave reaches the molten/hot zone before it solidifies.

$$t^* = \min(t_1^*, t_2^*) \tag{12}$$

$$\text{Trailing edge of the hot zone at that time, } x_1^* = V_{c,12}t_1^* - b = \frac{2V_{c,12}h_1(\rho_1S_1 - \rho_2S_2)}{\rho_2(S_1C_{02} - S_2C_{01})\cos\beta_1} - b \tag{13}$$

$$\text{Here, } V_{c,12} = \frac{U_{P,12}}{2\sin\left(\frac{\beta_2}{2}\right)} \tag{14}$$

For shock reflection to be critical, $x^* = 2h_1\tan\beta_1$

$$\frac{2V_{c,12}h_1(\rho_1S_1 - \rho_2S_2)}{\rho_2(S_1C_{02} - S_2C_{01})\cos\beta_1} - b \geq 2h_1\tan\beta_1 \tag{15}$$

Similarly, for the intermediate plate, $\frac{2V_{c,12}h_2(\rho_1 S_1-\rho_2 S_2)}{\rho_1(S_1 C_{02}-S_2 C_{01})\cos\beta_1} - b \geq 2h_2 \tan\beta_1$ (16)

Eq. 15 and Eq. 16 define when shock-induced tensile stress overlaps the hot zone, and the first among them to satisfy this will define the actual upper limit**.**
The maximum effective hot zone half-width $b_{1,max}$ is estimated from energy balance and thermal diffusion considerations as follows,

$$b_{1,max} = V_{c,12} \cdot \min(t_1^*, t_2^*) - 2h_1 \tan\beta_1 \quad (17)$$

Assuming an ideal conversion, where heat is required to reach the melting temperature of one of the materials at interface 1 is equal to the transferred kinetic energy converted to thermal energy over the hot zone. Therefore, the thermal energy input is defined as,

$$Q = \frac{1}{2} f \rho_1 h_1 V_1^2 \cdot V_{c,12} \quad (18)$$

Effective thermal properties are $k' = \frac{2k_1k_2}{k_1+k_2}$, $\alpha' = \frac{2\alpha_1\alpha_2}{\alpha_1+\alpha_2}$ (19)

The temperature rise in hot zone with width 2b becomes, $T_m = \frac{Qb}{k'\sqrt{\pi B}}$ (20)

Stress-wave arrival time = hot zone trailing edge position. f is the kinetic energy conversion factor, i.e. the fraction of the kinetic energy of the flyer being converted into thermal energy at the weld interface. Typical value 0.9 (i.e. 90% of energy).

$$B = \frac{h_1 V_{c,12}}{\alpha' \cos\beta\left(\frac{V_c}{U_{s1}} - \sin\beta_1\right)} \quad (21)$$

B is Dimensionless Thermal Strip Parameter, A thermal modeling parameter based on the moving strip heat source model. V_c Weld Velocity (Collision Front Speed)

$$V_c = \frac{V_i}{2\sin\left(\frac{\beta_1}{2}\right)} \quad (22)$$

Solve for V_i such that $T_m = \min(T_{m1}, T_{m2})$, V_i is the initial velocity of the flyer plate in its direction of travel at the moment of impact. Heat required to reach melt temp = Kinetic energy converted to thermal energy over a hot zone. Stress-wave arrival time = hot zone trailing edge position. Final symbolic expression

$$V_{i,max} = \sqrt{\frac{\min(T_{m1},T_{m,2})\cdot k'}{f' h_1^2 V_c}\left(\frac{V_c}{\min(U_{s1},U_{s2})\cos\beta_1} - \tan\beta_1\right)} \tag{23}$$

The shock velocity is now whichever arrives first. $U_s = \min(U_{s1}, U_{s2})$

$$V_{i,max} = 2.239\,\frac{\sqrt{k_1}\sqrt{k_2}\cdot(C_{01}+S_1U_{p1})^{\frac{1}{4}}\cdot\sqrt{\min(T_{m1},T_{m2})}\cdot\rho_2^{\frac{1}{4}}\cdot(\alpha_1+\alpha_2)^{1/4}}{V_c^{\frac{1}{4}}\cdot\sqrt{b}\cdot h_1^{\frac{1}{4}}\cdot\sqrt{\rho_1}\cdot\sqrt{k_1+k_2}\cdot\sqrt{f}\cdot(\alpha_1\alpha_2)^{\frac{1}{4}}}\cdot$$
$$\left(\frac{S_1C_{02}-S_2C_{01}}{(C_{01}\rho_2S_2\sin\beta_1 - C_{02}S_1\rho_2\sin\beta_1 + S_1V_c\rho_1 - S_2V_c\rho_2)\cos\beta_1}\right)^{\frac{1}{4}} \tag{24}$$

2.2.2 Interface 2: intermediate (plate 2) → target (plate 3)

Intermediate is now the new flyer, impacting the target at velocity $V_{impact,2\to3} \approx U_{p,12}$. Target is not massless and final interface has its own impedance, so shared velocity changes, So we must re-solve the Rankine-Hugoniot equations. Intermediate flyer velocity $= U_{p,12}$ and new shared particle velocity $U_{p,23}$

$$U_{P,23} = \frac{\rho_3C_{03}-\rho_2C_{02}}{(\rho_2S_2-\rho_3S_3)} \tag{25}$$

$$t_{delay} = \frac{d_{23}}{U_{P,12}} = \frac{d_{23}(\rho_1S_1-\rho_2S_2)}{\rho_2C_{02}-\rho_1C_{01}} \tag{26}$$

Shock Velocity Into Final Target (Plate 3), $U_{s3} = C_{03} + S_3U_{P,23} = C_{03} +$
$S_3\frac{\rho_3C_{03}-\rho_2C_{02}}{(\rho_2S_2-\rho_3S_3)} = \frac{\rho_2(S_2C_{03}-S_3C_{02})}{(\rho_2S_2-\rho_3S_3)}$ (27)

U_{s3} propagate into the target, reflect off the rigid base and return to interface 2. Another shock wave reflects back into plate 2, and a new wave re-enters plate 2. At interface 2, the intermediate plate (2) impacts the final target (3) after travelling a distance d_{23} at velocity $U_{P,12}$. Interact with the remaining molten zones between plates 1 and 2 at the interface. Possibly reflect off the flyer (plate 1) again, especially if it is still moving or elastic, which possibly adds to existing stress fields and causes secondary failure or delayed cracking at interface 1. We now compute whether the shock reflected from the back of the final target (plate 3) returns before solidification, causing dynamic cracking at the second interface.

$$t_3^* = \frac{d_{23}}{U_{P,12}} + \frac{2h_3}{U_{s3}\cos\beta_2}, \text{ here } V_{i,2} \approx U_{P,12} \tag{28}$$

$$V_{c,23} = \frac{U_{P,12}}{2\sin\left(\frac{\beta_2}{2}\right)} \tag{29}$$

Trailing edge of hot zone at that time,

$$x_3(t) = V_{c,23}t_3^* - b_2 = V_{c,23}\left(\frac{2h_3}{U_{s3}\cos\beta_2} + \frac{d_{23}(\rho_2 S_2 - \rho_3 S_3)}{\rho_3 C_{03} - \rho_2 C_{02}}\right) - b_2 \quad (30)$$

Similarly, for target shock reflection (critical melt crack distance) $x_3^* = 2h_2\tan\beta_2$

$$V_{c,23}\left(\frac{2h_3}{U_{s3}\cos\beta_2} + \frac{d_{23}(\rho_2 S_2 - \rho_3 S_3)}{\rho_3 C_{03} - \rho_2 C_{02}}\right) - b_2 \geq x_3^* = 2h_2\tan\beta_2 \quad (31)$$

As interface 2 involves a delayed collision between the deformable intermediate plate (Plate 2) and a rigidly backed target (Plate 3), $b_{2,max}$ can not be estimated using the same simplified geometric form as used for $b_{1,max}$,

$$b_{2,max} = V_{c,23}\cdot t_3^* - 2h_2\tan\beta_2 \quad (30) \quad (32)$$

The maximum allowable impact velocity $V_{i,2}$ at interface 2 based on thermal energy input and melting threshold - analogous to what was done for interface 1.

$$V_{i,2,max} = 2.239\frac{\sqrt{k_2}\sqrt{k_3}\cdot\sqrt{\min(T_{m1},T_{m2})}\cdot(\alpha_2+\alpha_3)^{1/4}}{V_{c,23}^{\frac{1}{4}}\cdot\sqrt{b_2}\cdot h_2^{\frac{1}{4}}\cdot\sqrt{\rho_2}\cdot\sqrt{k_2+k_3}\cdot\sqrt{f}\cdot(\alpha_2\alpha_3)^{\frac{1}{4}}}\left(\frac{S_2C_{03}-S_3C_{02}}{(C_{02}\rho_2S_3\tan\beta_2 - C_{03}S_2\rho_2\tan\beta_2 + S_2V_{c,23}\rho_2 - S_3V_{c,23}\rho_3)\cos\beta_2}\right)^{\frac{1}{4}} \quad (33)$$

When plate 2 impacts plate 3, a shock reflects back into plate 2, and may return to interface 1.

2.2.3 Shock return time (plate 2 → interface 1)

$$t_{return} = \left(\frac{2h_2}{U_{s2}\cos\beta_1}\right) \quad (34)$$

Where $U_{s2} = C_{02} + S_2U_{P,12}$. Now hot zone position and crack formation condition at interface 1 can be said as,

$$x(t_{return}) = V_{c,12}\cdot t_{return} - b_3 \quad (35)$$

$$V_{c,12}\left(\frac{2h_2}{U_{s2}\cos\beta_1}\right) - b_3 \geq 2h_1\tan\beta_1 \quad (36)$$

2.3 Smoothed particle hydrodynamics

SPH simulations were conducted using ANSYS Autodyn with a particle spacing of 5 μm to accurately resolve localized deformation and wave propagation in the multi-plate VFAW configuration. All plates were modeled using the Johnson-Cook plasticity model combined with a Grüneisen equation of state (EOS) to capture high-strain-rate plastic deformation and shock-induced thermal effects. Their constant values were taken from the literature. For validation, the flyer (Plate 1) was assigned an initial velocity of ~1400 m/s, estimated from the input energy (4 kJ) and foil mass (~8.1×10^{-5} kg). Boundary conditions included a fully clamped Plate 3 and a symmetric upper flyer. Thermo-mechanical coupling enabled the extraction of interfacial temperature fields and equivalent plastic strain and reflected shock interactions critical to weld evaluation and a qualitative validation of the analytical model.

3 Results and Discussion

The SPH simulations visually captured material flow and jetting behavior under oblique collision conditions. The initial impact at interface 1 produced localized plastic flow and jetting, as shown in Fig. 3 and as discussed through possible hypothesis in section 2.2. At interface 2 in Fig. 4, the SPH results effectively predicted critical shock return times and jetting criteria based on back-reflected stress waves, and the values are comparable with the analytical model, as also discussed through the possible analytical model. It was also interesting to observe that, contrary to available literature, minimal jetting was observed at interface 2.

The SPH results shown in Fig. 3 and Fig. 4 visualize the sequential shock dynamics within the three-plate assembly. The initial flyer impact creates a compressive wave at Interface 1, which then propagates through the intermediate plate (Plate 2) and drives a secondary collision with Plate 3. The resulting reflected wave from the rigidly backed target returns through Plate 2 and ultimately re-enters Plate 1. This behavior, captured in the time-resolved fringe patterns, confirms the mechanism hypothesized in our analytical model: that back-reflected shock waves may arrive at Interface 1 post-impact, potentially interfering with solidification and promoting late-stage cracking. The clear arrival timing agreement between SPH and predicted shock trajectories (Eq. 32–36) supports the validity of the proposed failure model. Notably, peak interfacial temperatures at Interface 1 exceeded 1200 K, and equivalent plastic strain localized near the jetting front surpassed 1.0, indicating severe plastic flow.

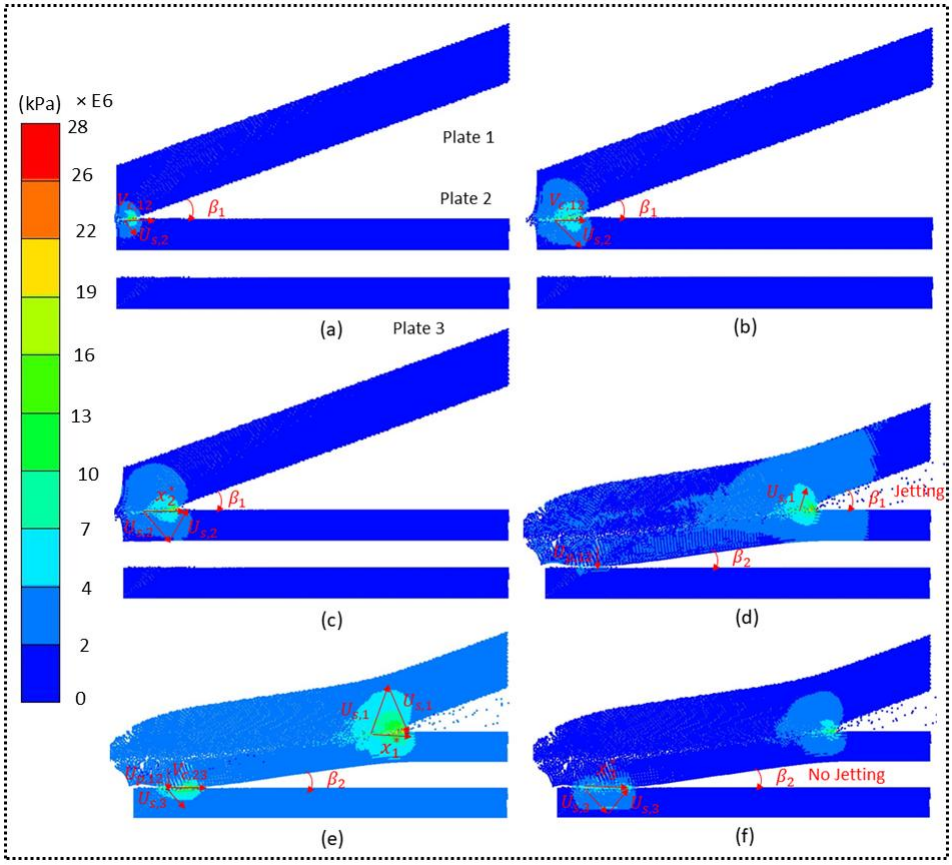

***Figure 3**: SPH modeling fringe pattern of shock wave showing oblique impact and material flow behavior during three-stack VFAW welding: (a–c) initial impact at interface 1 and (d–f) progressive impact at interface 2 (Eq. 1–14)*

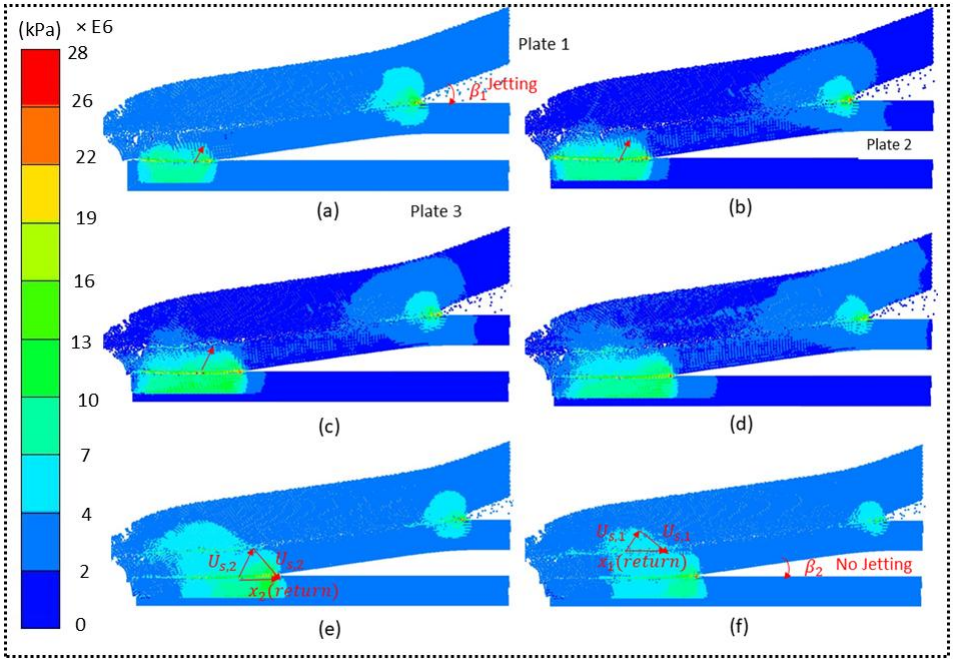

***Figure 4**: SPH modeling fringe pattern of shock wave reflections and return paths during three-stack VFAW welding: (a–e) shock generated at interface 2 propagates through plate 2 and returns to interface 1 and reflects back to interface 2 (as per Eq. 26–28); (d–f) extended shock wave traverses plate 1, partially reflects, and returns to interface 1 (Eq. 29–31)*

4 Conclusion

This work presents an integrated analytical and simulation-based study of 3-stack VFAW joints, emphasizing partial pre-forming and material flow dynamics. The proposed analytical framework captures critical physical mechanisms, including shock propagation and back-reflected wave effect, that govern weld quality and failure. SPH simulations complement the model by providing visual confirmation of interface behaviour of weldability as well as quantitative values of shock arrival time. Together, these approaches establish a predictive methodology for understanding and optimizing high-speed, multi-plate welding systems. In future work, we will enhance the analytical framework with machine learning-based surrogate modeling, train on SPH and experimental data, and elaborate on the multiphysics nature of the process. The hybrid analytical framework will be extended to experimentally calibrate process parameters and validate results through microstructural and mechanical testing of actual welds.

References

Yang, Y., Luo, Z., Zhang, Y. and Su, J., 2024. Dissimilar welding of aluminium to steel: a review. Journal of Manufacturing Processes, 110, pp.376-397.

Shi, L., Carlson, B.E., Li, S., Ghassemi-Armaki, H. and Li, G., 2025. Strengthening Mechanism of Aluminum Weld Nugget in Novel Dissimilar Resistance Spot Welds of AA5754 to Steels. Journal of Materials Engineering and Performance, pp.1-12.

Kumar, D., Kore, S.D. and Nandy, A., 2024. Electromagnetic joining for multi-material tubular components: a comprehensive review. International Journal of Precision Engineering and Manufacturing-Green Technology, 11(5), pp.1601-1636.

Kulkarni, M.R., Kolge, T., Kumar, D., Kore, S.D., Sharma, A., Srikanth, V., Laik, A., Chakraborty, G. and Albert, S., 2022. Magnetic pulse welding of D9 steel tube to SS316LN end plug. Transactions of the Indian Institute of Metals, pp.1-12.

Shi, L., Xue, J., Kang, J., Haselhuhn, A.S., Ghassemi-Armaki, H. and Carlson, B.E., 2023. Fatigue behavior of three-sheet aluminum-steel dissimilar resistance spot welds for automotive applications. Procedia Structural Integrity, 51, pp.102-108.

Achira, S., Abe, Y. and Mori, K.I., 2022. Self-pierce riveting of three thin sheets of aluminum alloy A5052 and 980 MPa steel. Materials, 15(3), p.1010.

Brechelt, S., Neef, P., Wiche, H. and Wesling, V., 2020. Spot weld bonding− process behavior of three-sheet steel stack-ups and analysis strategies with online measuring methods. Manufacturing Review, 7, p.3.

Vivek, A., Hansen, S.R., Liu, B.C. and Daehn, G.S., 2013. Vaporizing foil actuator: A tool for collision welding. Journal of Materials Processing Technology, 213(12), pp.2304-2311.

Kapil, A., Vivek, A. and Daehn, G., 2025. Role of zinc coating on joint properties in impact spot welded Al 6111 aluminum alloy to galvanized high-strength low-alloy steel. Journal of Advanced Joining Processes, 11, p.100276.

Kumar, D., Park, H.G., Choi, J., Kam, D.H., Lee, M. and Lee, T., 2025. The mechanical performance of the automotive Fe-Al dissimilar spot impact weld: In comparison to the self pierced riveted joint. International Journal of Fatigue, 193, p.108795.

Mao, Y., Thurson, B., Li, J., Vivek, A. and Daehn, G., 2021. High Strength Impact Welding of HSLA 340 to Al 5754 and Application Prototype. Universitätsbibliothek Dortmund.

Kapil, A., Mao, Y., Vivek, A., Cooper, R., Hetrick, E. and Daehn, G., 2020. A new approach for dissimilar aluminum-steel impact spot welding using vaporizing foil actuators. Journal of Manufacturing Processes, 58, pp.279-288.

Li, J., Vivek, A. and Daehn, G., 2021. Improved properties and thermal stability of a titanium-stainless steel solid-state weld with a niobium interlayer. Journal of Materials Science & Technology, 79, pp.191-204.

Liu, F., Guo, H., Chen, W., Zhang, X. and He, X., 2025. Experimental investigation of the mechanical properties of clinched joints in three-layer aluminium/SPCC steel/aluminium sheets. Materials Today Communications, p.111674.